

High-temperature lead-free multilayer ceramic capacitors with ultrahigh energy density and efficiency via fast two-step sintering

Supporting information

Ziming Cai^a, Chaoqiong Zhu^a, Hongxian Wang^a, Peiyao Zhao^a, Lingling Chen^a, Longtu Li^a, Xiaohui Wang^{a,*}

^aState Key Laboratory of New Ceramics and Fine Processing, School of Materials Science and Engineering, Tsinghua University, Beijing 100084, China

Corresponding Author

*Xiaohui Wang, E-mail: wxh@mail.tsinghua.edu.cn

1. Phase-field dielectric breakdown model

By drawing an analogy between dielectric breakdown and mechanical fracture, a scalar spatially and temporally dependent damage field $s(x, t)$ is introduced to characterize the breakdown process of a selected region of MLCCs.¹⁻³ The value of s varies from 1 to 0, representing the intact state and the fully damaged state, respectively. The fully damaged material becomes conductive. Numerically, a large but finite permittivity ε^0/η is taken for such material part, where ε^0 is the initial permittivity and η is a small enough number. For any other intermediate state of dielectric layer material, the permittivity is interpolated by

$$\varepsilon(s) = \frac{\varepsilon^0}{f(s) + \eta}, \quad (1)$$

where $f(s) = 4s^3 - 3s^4$. Breakdown happens if the process decreases the total potential energy of the system,

$$\Pi[s, \phi] = \int_{\Omega} [W_{es}(E, s) + W_d(s) + W_i(\nabla s)] dV, \quad (2)$$

where $W_{es}(E, s) = -\frac{\varepsilon}{2} E \cdot E$ is the complementary electrostatic energy per unit volume,

$W_d(s) = W_c[1 - f(s)]$ is the breakdown energy function with W_c representing the

critical density of electrostatic energy, $W_i(\nabla s) = \frac{\Gamma}{4} \nabla s \cdot \nabla s$ is the gradient energy term

to regulate sharp phase boundaries. Notably, the material parameter Γ is approximately

the breakdown energy. According to linear kinetic law: $\partial s / \partial t = -m \delta \Pi / \delta s$, the

evolution equation for breakdown variable s can be obtained after substituting in

detailed forms of the energy functions:

$$\frac{1}{m} \frac{\partial s}{\partial t} = \frac{\varepsilon'(s)}{2} \nabla \phi \cdot \nabla \phi + W_c f'(s) + \frac{\Gamma}{2} \nabla^2 s. \quad (3)$$

Here, mobility m is a material parameter that indicates the speed of breakdown

propagation in dielectric layers of MLCCs. By normalizing all lengths by l , energy

densities by W_c , time by $l^2 / m \Gamma$, and electric potential by $\sqrt{\Gamma / \varepsilon^0}$, the final normalized

governing equations of dimensionless form can be written as:

$$\nabla \cdot \left[\frac{1}{f(s) + \eta} \nabla \bar{\phi} \right] = 0, \quad (4)$$

$$\frac{\partial s}{\partial t} = - \frac{f'(s)}{2[f(s) + \eta]^2} \nabla \bar{\phi} \cdot \nabla \bar{\phi} + f'(s) + \frac{1}{2} \nabla^2 s, \quad (5)$$

in which the corresponding quantities are symbolized with over-bars. The dielectric

breakdown behavior of MLCCs can be simulated by implementing the normalized

governing equations (4) and (5) into COMSOL Multiphysics platform. The voltage

between two electrodes is applied quasi-statically by controlling the total charge

accumulation of the negative electrode.

2. Microstructure and electrical properties of MLCCs sintered with various first-step heating rate

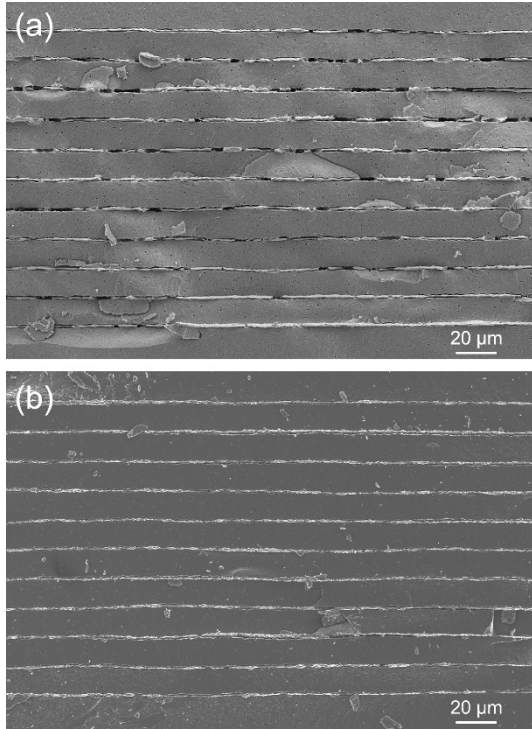


Figure S1. Large-view cross-sectional SEM images of the MLCCs sintered with the first-step heating rate of (a) 4 °C/min, (b) 40 °C/min, in which the pores and discontinuity of internal electrodes can be distinguished more clearly.

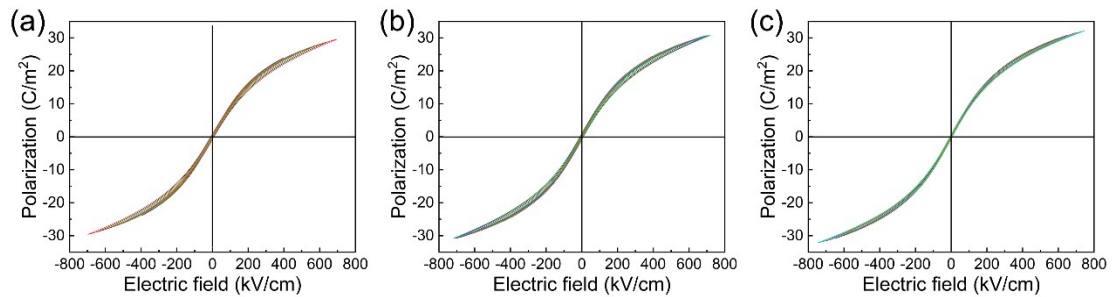


Figure S2. Hysteresis loops of MLCCs sintered with the first-step heating rate of (a) 4 °C/min, (b) 20 °C/min, (c) 40 °C/min, measured under various applied electric field at

1Hz.

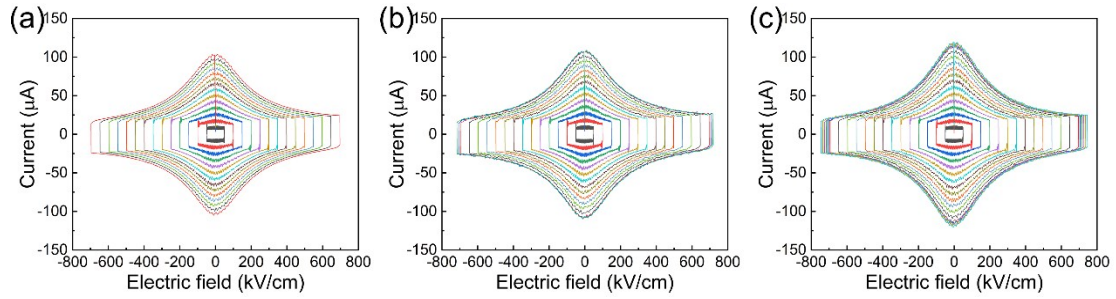


Figure S3. The current-electric-field relation of MLCCs sintered with the first-step heating rate of (a) 4 °C/min, (b) 20 °C/min, (c) 40 °C/min, measured under various applied electric field at 1Hz, corresponding to Figure S2.

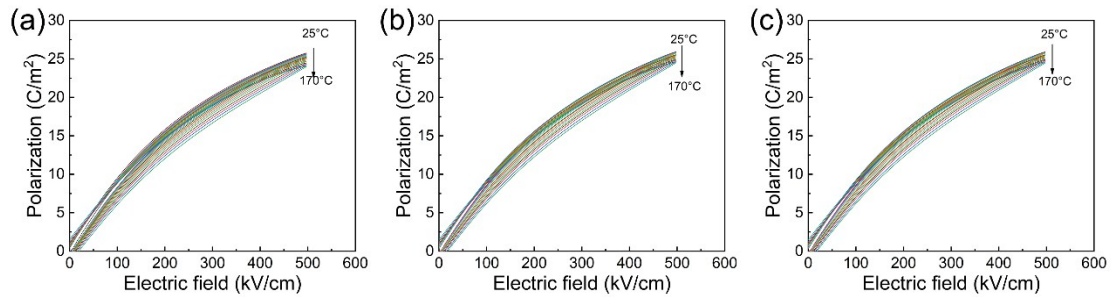


Figure S4. The temperature-dependent unipolar hysteresis loop the MLCCs sintered with the first-step heating rate of (a) 4 °C/min, (b) 20 °C/min, (c) 40 °C/min, measured under the maximum electric field of 500 kV/cm at 1 Hz.

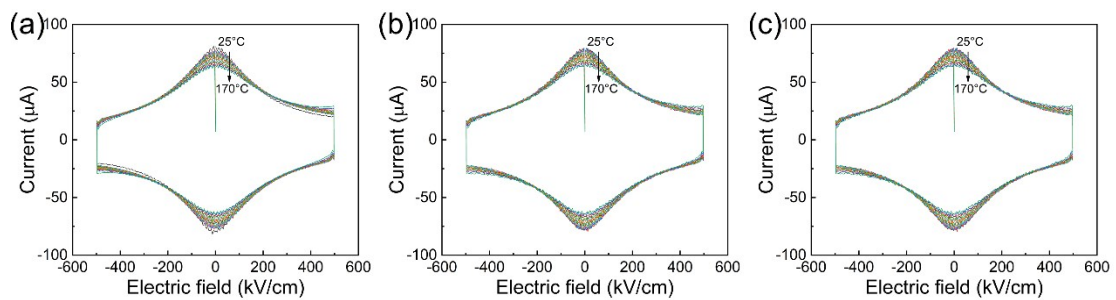


Figure S5. The temperature-dependent current-electric-field relation the MLCCs sintered with the first-step heating rate of (a) 4 °C/min, (b) 20 °C/min, (c) 40 °C/min, measured under the maximum electric field of 500 kV/cm at 1 Hz, corresponding to Figure S4.

Table S1. The insulation resistivity of the MLCCs with various first-step heating rate of 4 °C/min (MLCC-4), 20 °C/min (MLCC-20) and 40 °C/min (MLCC-40).

Samples	Insulation resistivity ($\times 10^{11} \Omega m$)
MLCC-4	5.92
MLCC-20	11.6
MLCC-40	63.6

3. Two-step sintering method

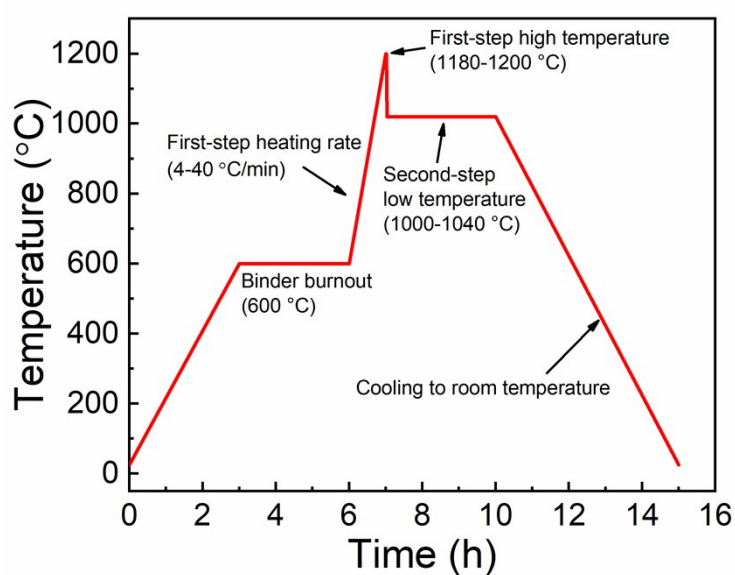


Figure S6. The two-step sintering schedule of MLCCs with the first-step heating rate of 4 °C/min, 20 °C/min and 40 °C/min, respectively.

References:

1. K. C. Pitike and W. Hong, *J. Appl. Phys.*, 2014, **115**, 044101.
2. Z. Cai, X. Wang, B. Luo, W. Hong, L. Wu and L. Li, *Compos. Sci. Technol.*, 2017, **151**, 109-114.
3. Z. Cai, X. Wang, B. Luo, W. Hong, L. Wu and L. Li, *Compos. Sci. Technol.*, 2017, **145**, 105-113.